



Anomalous grain growth in sintered $\text{Bi}_2\text{Ca}_2\text{Co}_{2-x}\text{Cu}_x\text{O}_y$ + Ag ceramic composites by Cu doping

H. Amaveda¹, M. A. Madre¹, M. Mora¹, M. A. Torres¹, and A. Sotelo^{2,1,*}

¹Instituto de Nanociencia y Materiales de Aragón (CSIC-Universidad de Zaragoza), M^a de Luna, 3, 50018 Zaragoza, Spain

²Dept. Ciencia de Materiales, C/M^a de Luna, 3, 50018 Zaragoza, Spain

Received: 25 May 2022

Accepted: 24 October 2022

Published online:

7 January 2023

© The Author(s) 2023

ABSTRACT

$\text{Bi}_2\text{Ca}_2\text{Co}_{2-x}\text{Cu}_x\text{O}_y$ + 4 wt%Ag (with x between 0 and 0.20) thermoelectric materials were prepared through a sol-gel method via nitrates. Powder XRD patterns showed the presence of thermoelectric phase as the major one, accompanied by metallic silver. SEM observations identified three different secondary phases in the samples, together with an exaggerated grain growth with Cu doping. The microstructural modifications are reflected in an important decrease of electrical resistivity, $\sim 3\%$ when compared to undoped samples, due to the reduction on the number of grain boundaries, and the increase of Co^{4+} in the conducting layer. The minimum values at 650 °C were obtained in 0.10 Cu-doped samples, 69 mΩ cm, which are lower than the reported in sintered samples. On the other hand, Seebeck coefficient was only slightly affected and reached the highest values at 650 °C in 0.15 Cu-doped samples, 215 μV/K, which is practically the same measured in undoped ones, 211 μV/K, and lower than those reported for sintered samples. Consequently, the highest PF at 650 °C has been determined in 0.10 Cu-doped samples, which is around 50% higher than the obtained in samples prepared through the classical solid-state method, or the undoped ones prepared in this work.

1 Introduction

In the present world situation, with the drastic increase of energy prices and the involvement of governments to fight against global warming, the search for more sustainable energy sources is drastically increased. For this purpose, thermoelectric (TE) materials with high energy conversion efficiency are strongly required for electric power generation from

renewable sources [1–3] or by harvesting the wasted heat in other energy transformations systems [4, 5]. The evaluation of performances of these materials is usually performed through the so-called dimensionless figure of merit, ZT, where the Seebeck coefficient (S), absolute temperature (T), electrical resistivity (ρ), and thermal conductivity (κ) are correlated in the form [6]: $ZT = TS^2/\rho\kappa$. Consequently, a good thermoelectric material should have high Seebeck coefficient and working temperatures, with low electrical resistivity, and thermal conductivity.

Address correspondence to E-mail: asotelo@unizar.es

<https://doi.org/10.1007/s10854-022-09416-x>

Nowadays, the highest ZT values are obtained in intermetallic compounds, such as CoSb_3 or Bi_2Te_3 [7, 8], with medium-low working temperatures and drawbacks associated with possible oxidation or degradation when they are exposed at high temperatures. Moreover, they are usually composed by scarce [9, 10], heavy, and/or toxic elements with relatively high environmental impact. These limitations have been started to be surpassed in 1997 with the discovery of relatively high thermoelectric performances in a ceramic material: Na_xCoO_2 [11]. This discovery has been the milestone to start a large research activity in the field of thermoelectric ceramics. From this activity, it has been found that many CoO-based materials display promising thermoelectric properties, such as $\text{Ca}_3\text{Co}_4\text{O}_9$, $\text{Bi}_2\text{Sr}_2\text{Co}_2\text{O}_y$, or $\text{Bi}_2\text{Ca}_2\text{Co}_2\text{O}_y$ [12–15]. These materials are usually known as misfit cobaltites due to their crystal structure, which can be described through a monoclinic system composed of two different layers alternatively stacked. These layers are a common conductive CdI_2 -type CoO_2 layer with a two-dimensional triangular lattice and an insulating block one, with rock-salt-type (RS) structure. Both layers possess the same a- and c-axis lattice parameters and β angles, but they differ in the b-axis length, responsible of the misfit along this direction [16, 17]. Furthermore, this crystal structure leads to strong crystallographic anisotropy, which is reflected on the grain shapes due to their preferential grain growth along the ab-planes, leading to platelike shaped grains with strongly anisotropic properties. Consequently, the orientation of these grains along a preferential direction is shown as crucial to maximize the properties of these compounds.

Some processes have been successfully used to obtain good grain orientation in this family of compounds, such as template grain growth (TTG) [17], sinter-forging [18], spark plasma [19], or directional growth from the melt [20]. Moreover, cationic substitutions can also modified the $\text{Co}^{3+}/\text{Co}^{4+}$ relationship in the conducting layer, allowing controlled modifications on the charge carrier concentration and, consequently, on the thermoelectric properties of these samples [21, 22], in agreement with Koshi-bae's equation [23]. Finally, the use of noble metal additions has also shown to improve the thermoelectric properties of these compounds by enhancing intergranular connectivity [24].

Taking into account the previously discussed effects, the aim of this work is producing high-performances Cu-doped $\text{Bi}_2\text{Ca}_2\text{Co}_2\text{O}_y + 4 \text{ wt\% Ag}$ TE materials prepared by the sol-gel method via nitrates in order to avoid the necessity of expensive equipment and/or long processes.

2 Experimental

The initial $\text{Bi}_2\text{Ca}_2\text{Co}_{1-x}\text{Cu}_x\text{O}_y + 4 \text{ wt\% Ag}$ ($x = 0.0, 0.03, 0.05, 0.1, 0.15, \text{ and } 0.20$) polycrystalline ceramics were prepared using commercial $\text{Bi}(\text{NO}_3)_3 \cdot 5\text{H}_2\text{O}$ ($\geq 98\%$, Aldrich), CaCO_3 (98.5%, Panreac), $\text{Co}(\text{NO}_3)_2 \cdot 6\text{H}_2\text{O}$ (98%, Panreac), CuO (98%, Panreac), and metallic Ag (99%, Aldrich) powders through a sol-gel method. The powders were weighed in the stoichiometric proportions and added to a mixture of HNO_3 (analysis grade, Panreac) and double distilled water to be dissolved in the form of nitrates, leading to a clear pink solution. To this solution, citric acid (99.5%, Panreac) and ethylene glycol (99%, Panreac) were added in the appropriate proportions. After mixing in a magnetic stirrer for 30 min at 300 rpm, the solution was heated at 80°C to slowly evaporate the solvent and decompose the HNO_3 excess. The nitric acid decomposition modifies the solution pH, leading to the polymerization reaction between citric acid and ethylene glycol, producing a pink gel with the different cations coordinated to the resulting polymer [25, 26]. Further heating at around 350°C produces the self-combustion of the gel, producing a very fine brownish powder, composed of a mixture of oxides and carbonates. The resulting powder was manually milled and thermally treated in two steps, at 700 and 750°C for 12 h each one, with an intermediate manual grinding, to decompose the carbonates and start forming some intermediate phases. Finally, the calcined powders were cold uniaxially pressed in the form of pellets ($3 \times 3 \times 15 \text{ mm}^3$) under an applied pressure of about 400 Mpa for 1 min, and sintered at 750°C for 24 h with a final furnace cooling.

All samples were structurally characterized by powder XRD utilizing a Rigaku D/max-B X-ray powder diffractometer ($\text{CuK}\alpha$ radiation) with 2θ ranging between 5 and 40 degrees. Microstructural observations were performed on the samples surfaces using a Field Emission Scanning Electron Microscope (FESEM, Carl Zeiss Merlin), with energy-dispersive

spectrometry (EDS) analysis. Simultaneous measurements of resistivity and Seebeck coefficient were determined in steady-state mode through the standard dc four-probe configuration in a LSR-3 system (Linseis GmbH) at temperatures ranging between 50 and 650 °C under protective He atmosphere. Finally, using electrical resistivity and Seebeck coefficient data, power factor ($PF = S^2/\rho$) was calculated to determine the electrical performances of these samples as a function of temperature and Cu doping.

3 Results and discussion

Powder XRD patterns for all $\text{Bi}_2\text{Ca}_2\text{Co}_2-x\text{Cu}_x\text{O}_y + 4$ wt%Ag samples are presented in Fig. 1. As it can be observed in the graph, all samples show very similar patterns, and the most intense peaks are associated with the thermoelectric phase, in agreement with previous reported data [27]. Moreover, it can be also observed a small peak at around 38.5 degrees (indicated by #), associated with the (111) reflection of metallic Ag [28, 29]. Consequently, it can be deduced that samples are composed of single thermoelectric phase accompanied by metallic Ag. This result clearly confirms that Ag does not react with the

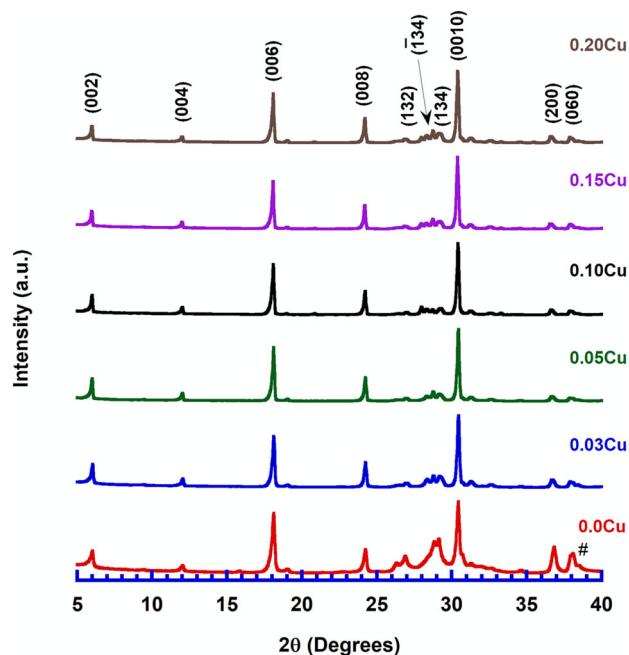


Fig. 1 Powder XRD diagrams for the $\text{Bi}_2\text{Ca}_2\text{Co}_2-x\text{Cu}_x\text{O}_y + 4$ wt% Ag samples. Crystallographic planes identify the peaks corresponding to the thermoelectric phase. # symbol shows the (111) peak of Ag

thermoelectric phase, as observed in similar systems, even if they are melt processed [30, 31].

Scanning electron microscopy has been performed on the surfaces of all samples, and representative micrographs, taken using backscattered electrons, are presented in Fig. 2. In these images, it can be clearly seen that all samples present a random orientation of grains, typical configuration for classically sintered samples. Moreover, Cu doping promotes a drastic and anomalous increase of grain sizes, when compared to those observed in the undoped samples. This effect is due to the formation of an eutectic $\text{Bi}_2\text{O}_3\text{--CuO}$ which melts at around 770 °C [32] and increases cation mobility. On the other hand, Cu doping also leads to the formation of different contrasts (numbered for clarity) in the micrographs, which have been analyzed through EDS to determine their semi-quantitative chemical composition. They are gray (#1) $\text{Bi}_2\text{Ca}_2\text{Co}_2-x\text{Cu}_x\text{O}_y$ thermoelectric phase; white (#2) Bi_3CaO_z ; black (#3) Co oxide; and light gray (#4) $\text{Bi}_5\text{CaCoO}_w$, in agreement with the phase equilibria diagram for the Bi–Ca–Co–O system [33] Furthermore, Ag has also been identified as very small particles in micrographs obtained at higher magnifications. All these secondary phases have not been found through the XRD technique. The reason can be associated with different factors: the small amount of these secondary phases and/or the large enhancement of the (00 L) peaks of the thermoelectric phase due to the preferential orientation of grains during powder sample preparation for the XRD analysis, as previously observed [34].

The evolution of the electrical resistivity with temperature as a function of the Cu content is represented in Fig. 3. In the graph, it is very clear that Cu doping leads to the decrease of electrical resistivity, which can be associated with several factors. One is the increase of grain sizes, producing a decrease of the number of grain boundaries, which are known to be more resistive than the grains. Another factor is the substitution of Co^{3+} by Cu^{2+} which should promote some part of the Co^{3+} in the conducting layer to Co^{4+} to maintain the electrical neutrality. As a consequence, the charge carrier concentration is increased, leading to enhanced electrical conductivities. On the other hand, when observing the electrical resistivity variation with Cu content, it is easy to see that it decreases for Cu doping up to 0.10, increasing

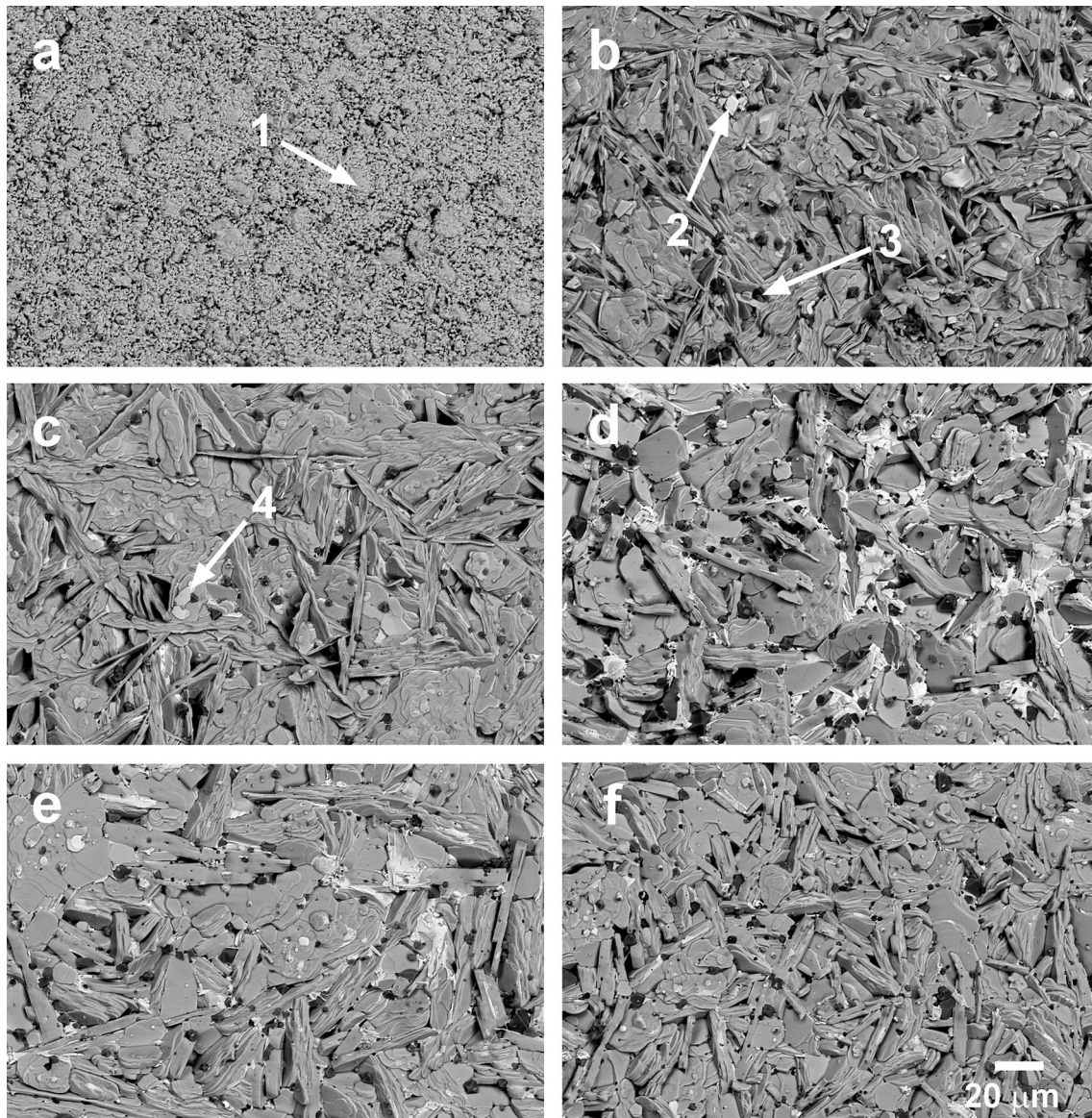


Fig. 2 Representative SEM micrographs obtained in the samples surfaces. The different phases are indicated by numbers: (#1) $\text{Bi}_2\text{Ca}_2\text{Co}_2 - x\text{Cu}_x\text{O}_y$ thermoelectric phase; (#2) Bi_3CaO_2 ; (#3) Co oxide; and (#4) $\text{Bi}_5\text{CaCoO}_w$

for higher content. This increase is due to the competitive effect of defect introduction when Cu is present in the samples, which scatters charge carriers and tends to increase electrical resistivity. The combination of grain growth, increase of charge carrier concentration, and increase of crystal defects can explain the electrical resistivity evolution with Cu content. The minimum values at 650°C have been measured in 0.10 Cu-substituted samples ($69\text{ m}\Omega\text{ cm}$), which is lower than the reported for laser-textured materials ($80\text{--}85\text{ m}\Omega\text{ cm}$) [26], or sintered materials produced through the classical solid-state method ($120\text{ m}\Omega\text{ cm}$) [35]. On the other hand, they are

higher than those measured in textured materials using platelet seeds or by hot uniaxial pressing along the ab-plane ($22\text{ m}\Omega\text{ cm}$) [36, 37], and the published results for sintered samples produced by soft chemistry methods ($40\text{ m}\Omega\text{ cm}$) [35].

Figure 4 displays the variation of the Seebeck coefficient with temperature, as a function of Cu doping. In the graph, it is clear that Seebeck coefficient shows positive sign in the whole measured temperature range. This fact confirms that these samples display a hole-dominant conduction mechanism. Moreover, the Seebeck coefficient values are

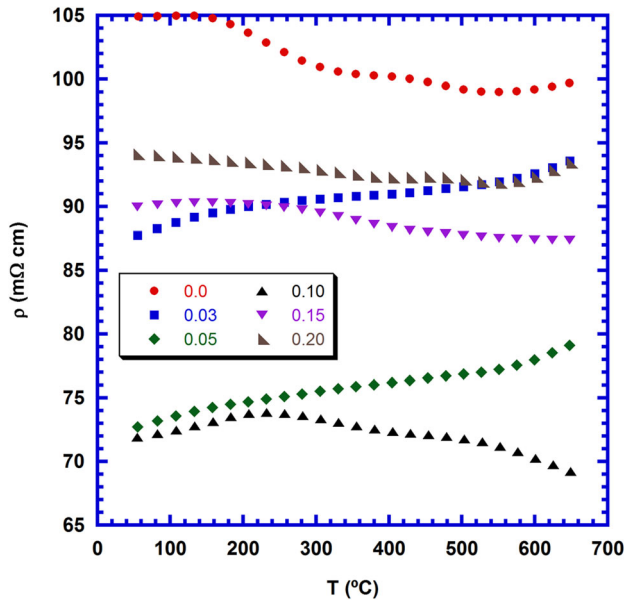


Fig. 3 Temperature dependence of the electrical resistivity for sintered $\text{Bi}_2\text{Ca}_2\text{Co}_{2-x}\text{Cu}_x\text{O}_y + 4 \text{ wt\% Ag}$, as a function of Cu content

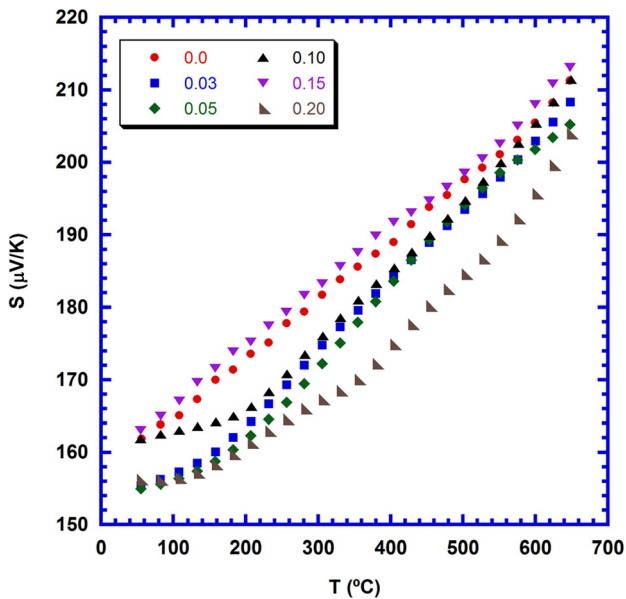


Fig. 4 Temperature dependence of the Seebeck coefficient for sintered $\text{Bi}_2\text{Ca}_2\text{Co}_{2-x}\text{Cu}_x\text{O}_y + 4 \text{ wt\% Ag}$, as a function of Cu content

increased with temperature, which is in agreement with the typical behavior of metals or degenerated semiconductors when the variation of different parameters with temperature, as carrier concentration, effective mass, and Fermi level, are negligible [24]. The highest measured values at 650 °C correspond to the 0.15 Cu-doped samples (215 $\mu\text{V/K}$),

which are higher of the reported for laser-textured materials (170 $\mu\text{V/K}$) [26], and in the order of those obtained in materials produced through the classical solid-state method (225 $\mu\text{V/K}$) [35], or textured using platelet seeds or by hot uniaxial pressing (240 $\mu\text{V/K}$) [36, 37].

The performances of these materials have been evaluated through the power factor, calculated from the electrical resistivity and Seebeck coefficient data, and displayed, as a function of Cu doping, in Fig. 5. As it was observed in the Seebeck coefficient graph (see Fig. 4), Cu doping leads to only slight differences between the samples. On the other hand, it leads to more important variations in electrical resistivity. Consequently, the differences in power factor will be mainly due to the electrical resistivity values, and the highest PF values have been obtained in the 0.10 Cu-doped samples, which displayed the minimum electrical resistivity in the whole measured temperature range. At 650 °C, the maximum value has been 0.065 $\text{mW/K}^2 \text{ m}$, which is around 50% higher than that obtained in undoped samples or in classically sintered ones (0.042 $\text{mW/K}^2 \text{ m}$) [35]. On the other hand, it is slightly lower than the reported for laser-textured materials (0.085 $\text{mW/K}^2 \text{ m}$) [26], and much lower than those reported for hot pressed ceramics (0.25 $\text{mW/K}^2 \text{ m}$) [37]. Even if these values are still low when compared to textured materials, the samples

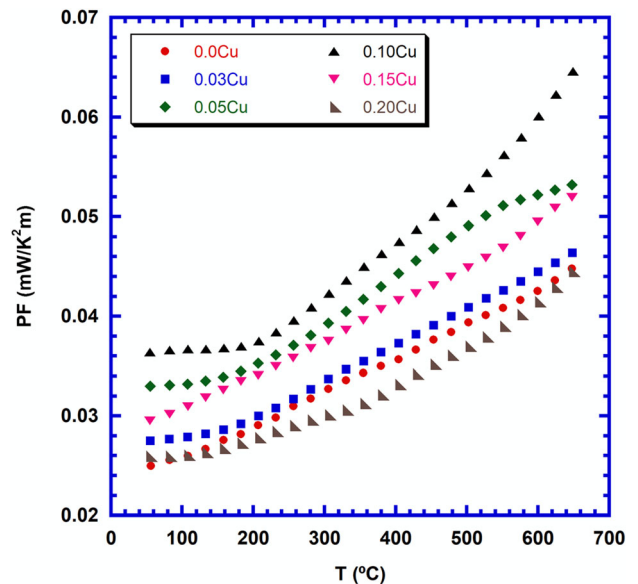


Fig. 5 Temperature dependence of the power factor for sintered $\text{Bi}_2\text{Ca}_2\text{Co}_{2-x}\text{Cu}_x\text{O}_y + 4 \text{ wt\% Ag}$, as a function of Cu content

studied in this work are produced using an easily scalable and economic process, which avoids the use of long processes and expensive equipment.

Finally, despite the enhancement of thermoelectric properties by Cu doping, it should be considered that too large grain sizes are not mechanically desirable in compounds with platelike grains, as they are weakly bonded along their *c*-axis. These characteristics lead to cracks formation perpendicularly to this axis between these large grains, as observed in similar systems [38], compromising the mechanical integrity of thermoelectric modules.

4 Conclusion

In this work, $\text{Bi}_2\text{Ca}_2\text{Co}_2 - x\text{Cu}_x\text{O}_y + 4 \text{ wt}\% \text{Ag}$ ($0 \leq x \leq 0.20$) thermoelectric materials have been prepared by the sol-gel method via nitrates. Powder XRD patterns showed the thermoelectric phase as the major one, accompanied by metallic silver, and no evidence of secondary phases has been found. SEM microstructural observations allowed identifying three different secondary phases, and noting an unusual and drastic grain growth with Cu doping. These changes in microstructure have been reflected in a significant decrease of electrical resistivity, $\sim 30\%$ when compared to undoped samples, due to the reduction on the number of grain boundaries, and an increase of charge carrier concentration. The minimum values have been achieved in 0.10 Cu-doped samples at 650 °C, 69 mΩ cm, which are lower than the reported in samples with randomly oriented grains. On the other hand, their effect on the Seebeck coefficient values is very limited. The highest values have been determined in 0.15 Cu-doped samples, 215 μV/K, which is slightly higher than the measured in undoped ones, 211 μV/K, and lower than those reported for samples formed by grains without preferential orientation. Consequently, the highest PF at 650 °C has been determined in 0.10 Cu-doped samples, around 50% higher than the obtained in samples prepared through the classical solid-state method, or the undoped ones prepared in this work.

All these results clearly indicate that the use of Cu electrodes in thermoelectric modules is undesirable, as Cu can diffuse within the thermoelectric compound at working temperatures, leading to an undesirable and exaggerated grain growth.

Acknowledgements

The Authors would like to acknowledge the use of Servicio General de Apoyo a la Investigación-SAI, Universidad de Zaragoza.

Author contributions

All authors contributed equally to the present study. MM and HA prepared the samples; MAT performed the thermoelectric characterization; MAM made the microstructural characterization; and AS prepared the draft. All authors have collaborated to produce the final version of the manuscript.

Funding

Open Access funding provided thanks to the CRUE-CSIC agreement with Springer Nature. This research has been supported by the Spanish MINECO-FEDER project (Grant No. MAT2017-82183-C3-1-R) and the Aragón Government (Research Group T54-20R).

Data availability

Data cannot be made available, as it is part of an ongoing study.

Declarations

Conflict of interest The authors have no relevant financial or non-financial interests to disclose.

Open Access This article is licensed under a Creative Commons Attribution 4.0 International License, which permits use, sharing, adaptation, distribution and reproduction in any medium or format, as long as you give appropriate credit to the original author(s) and the source, provide a link to the Creative Commons licence, and indicate if changes were made. The images or other third party material in this article are included in the article's Creative Commons licence, unless indicated otherwise in a credit line to the material. If material is not included in the article's Creative Commons licence and your intended use is not permitted by statutory regulation or exceeds the permitted use, you will need to obtain permission

directly from the copyright holder. To view a copy of this licence, visit <http://creativecommons.org/licenses/by/4.0/>.

References

- W. Liu, X. Yan, G. Chen, Z. Ren, Recent advances in thermoelectric nanocomposites. *Nano Energy* **1**, 42–56 (2012)
- A. Nozariasbmarz, H. Collins, K. Dsouza, M.H. Polash, M. Hosseini, M. Hyland, J. Liu, A. Malhotra, F.M. Ortiz, F. Mohaddes, V.P. Ramesh, Y. Sargolzaeiaval, N. Snouwaert, M.C. Ozturk, D. Vashae, Review of wearable thermoelectric energy harvesting: from body temperature to electronic systems. *Appl. Energy* **258**, 114069 (2020)
- L. Sigrist, N. Stricker, D. Bernath, J. Beutel, L. Thiele, Thermoelectric energy harvesting from gradients in the Earth Surface. *IEEE Trans. Ind. Electron.* **67**, 9460–9470 (2020)
- M.H. Elsheikh, D.A. Shnawah, M.F.M. Sabri, S.B.M. Said, M.H. Hassan, M.B.A. Bashir, M. Mohamad, A review on thermoelectric renewable energy: Principle parameters that affect their performance. *Renew. Sust Energy Rev.* **30**, 337–355 (2014)
- S. LeBlanc, Thermoelectric generators: linking material properties and systems engineering for waste heat recovery applications. *Sust Mater. Technol.* **1–2**, 26–35 (2014)
- D.M. Rowe, in *Thermoelectrics handbook: macro to nano*, 1st edn., ed. by D.M. Rowe (CRC Press, Boca Raton, 2006), pp.1-3–1-7
- J.A. Santamaria, J. Alkorta, J.G. Sevillano, Microcompression tests of single-crystalline and ultrafine grain Bi₂Te₃ thermoelectric material. *J. Mater. Res.* **30**, 2593–2604 (2015)
- H. Wang, J. Hwang, M.L. Snedaker, I.-H. Kim, C. Kang, J. Kim, G.D. Stucky, J. Bowers, W. Kim, High thermoelectric performance of a heterogeneous PbTe nanocomposite. *Chem. Mater.* **27**, 944–949 (2015)
- A.A. Yaroshevsky, Abundances of chemical elements in the earth's crust. *Geochem. Int.* **44**, 48–55 (2006)
- J. He, Y. Liu, R. Funahashi, Oxide thermoelectrics: the challenges, progress, and outlook. *J. Mater. Res.* **26**, 1762–1772 (2011)
- I. Terasaki, Y. Sasago, K. Uchinokura, Large thermoelectric power in NaCo₂O₄ single crystals. *Phys. Rev. B* **56**, 12685–12687 (1997)
- A.C. Masset, C. Michel, A. Maignan, M. Hervieu, O. Toulemonde, F. Studer, B. Raveau, J. Hejtmanek, Misfit-layered cobaltite with an anisotropic giant magnetoresistance: Ca₃Co₄O₉. *Phys. Rev. B* **62**, 166–175 (2000)
- H. Leligny, D. Grebille, O. Perez, A.C. Masset, M. Hervieu, B. Raveau, A five-dimensional structural investigation of the misfit layer compound [Bi_{0.87}SrO₂]₂[CoO₂]_{1.82}. *Acta Cryst B* **56**, 173–182 (2000)
- A. Maignan, D. Pelloquin, S. Hebert, Y. Klein, M. Hervieu, Thermoelectric power in misfit cobaltites ceramics: optimization by chemical substitutions. *Bol. Soc. Esp. Ceram. V.* **45**, 122–125 (2006)
- W. Kobayashi, S. Hebert, H. Muguerra, D. Grebille, D. Pelloquin, A. Maignan, Thermoelectric properties in the misfit-layered-cobalt oxides [Bi₂A₂O₄][CoO₂]_{b1/b2} (A = Ca, Sr, Ba, b(1)/b(2) = 1.65, 1.82, 1.98) single crystals. In I. Kim (Ed.), *Proceedings ICT 07: Twenty-sixth international conference on thermoelectrics, Korea*, (2008), pp. 117–120
- A. Maignan, S. Hebert, M. Hervieu, C. Michel, D. Pelloquin, D. Khomskii, Magnetoresistance and magnetothermopower properties of Bi/Ca/Co/O and Bi(Pb)/Ca/Co/O misfit layer cobaltites. *J. Phys.* **15**, 2711–2723 (2003)
- H. Itahara, C. Xia, J. Sugiyama, T. Tani, Fabrication of textured thermoelectric layered cobaltites with various rock salt-type layers by using b-Co(OH)₂ platelets as reactive templates. *J. Mater. Chem.* **14**, 61–66 (2004)
- W. Shin, N. Murayama, Thermoelectric properties of (Bi,Pb)-Sr-Co-O oxide. *J. Mater. Res.* **15**, 382–386 (2000)
- J.G. Noudem, D. Kenfaui, D. Chateigner, M. Gomina, Toward the enhancement of thermoelectric properties of lamellar Ca₃Co₄O₉ by edge-free spark plasma texturing. *Scripta Mat.* **66**, 258–260 (2012)
- A. Sotelo, E. Guilmeau, M.A. Madre, S. Marinel, J.C. Diez, M. Prevel, Fabrication and properties of textured bi-based cobaltite thermoelectric rods by zone melting. *J. Eur. Ceram. Soc.* **27**, 3697–3700 (2007)
- H.Q. Liu, X.B. Zhao, T.J. Zhu, Y. Song, F.P. Wang, Thermoelectric properties of Gd, Y co-doped Ca₃Co₄O_{9+δ}. *Curr. Appl. Phys.* **9**, 409–413 (2009)
- G. Constantinescu, Sh. Rasekh, M.A. Torres, P. Bosque, M.A. Madre, A. Sotelo, J.C. Diez, Thermoelectric doping effect in Ca₃Co_{4-x}Ni_xO₉ ceramics. *Bol. Soc. Esp. Ceram. V.* **54**, 21–27 (2015)
- W. Koshibae, K. Tsutsui, S. Maekawa, Thermopower in cobalt oxides. *Phys. Rev. B* **62**(11), 6869–6872 (2000)
- D. Flahaut, J. Allouche, A. Sotelo, Sh Rasekh, M.A. Torres, M.A. Madre, J.C. Diez, Role of Ag in textured-annealed Bi₂Ca₂Co_{1.7}O_x thermoelectric ceramic. *Acta Mater.* **102**, 273–283 (2016)
- Z. Gaoke, L. Ying, Y. Xia, W. Yanping, O. Shixi, L. Hangxing, Comparison of synthesis methods, crystal structure and characterization of strontium cobaltite powders. *Mater. Chem. Phys.* **99**, 88–95 (2006)
- M.A. Sh. Rasekh, A. Madre, E. Sotelo, S. Guilmeau, J.C. Marinel, Diez, Effect of synthetic methods on the

- thermoelectrical properties of textured $\text{Bi}_2\text{Ca}_2\text{Co}_{1.7}\text{O}_x$ ceramics. *Bol. Soc. Esp. Ceram. V.* **49**, 89–94 (2010)
27. E. Guilmeau, M. Pollet, D. Grebille, D. Chateigner, B. Vertruyen, R. Cloots, R. Funahashi, Neutron diffraction texture analysis and thermoelectric properties of BiCaCoO misfit compounds. *Mater. Res. Bull.* **43**, 394–400 (2008)
 28. H.E. Swanson, E. Tatge, Standard X-ray diffraction powder patterns. *Natl. Bureau Stand. Circ.* **539**, 1–95 (1953)
 29. G. Becherer, R. Ifland, Über eine präzisionsbestimmung der gitterkonstanten von silber nach dem rückstrahlverfahren. *Naturwissenschaft* **41**, 471–471 (1954)
 30. A. Sh. Rasekh, M.A. Sotelo, P. Torres, M.A. Bosque, J.C. Madre, Diez, Thermoelectric properties of directionally grown $\text{Bi}_2\text{Ba}_2\text{Co}_2\text{O}_8/\text{Ag}$ composites: effect of annealing. *J. Mater. Sci.* **27**, 12964–12973 (2016)
 31. B. Rivas-Murias, H. Muguerra, M. Traianidis, C. Henrist, B. Vertruyen, R. Cloots, Enhancement of the power factor of $[\text{Bi}_{1.68}\text{Ca}_2\text{O}_4]^{\text{RS}}[\text{CoO}_2]_{1.69}$ – ag composites prepared by the spray-drying method. *Solid State Sci.* **12**, 1490–1495 (2010)
 32. Yu.F. Kargin, V.M. Skorikov, Bi_2O_3 -CuO system. *Russ J. Inorg. Chem.* **34**, 1552–1553 (1989)
 33. A.I. Klyndyuk, N.S. Krasutskaya, I.V. Matsukevich, E.A. Tugova, E.A. Chizhova, Phase equilibria in the $\text{BiO}_{1.5}$ -CaO- CoO_y system. *Russ J. Gen. Chem.* **88**, 1063–1065 (2018)
 34. H. Muguerra, B. Rivas-Murias, M. Traianidis, C. Henrist, B. Vertruyen, R. Cloots, Improvement of the thermoelectric properties of $[\text{Bi}_{1.68}\text{Ca}_2\text{O}_{4-\delta}]^{\text{RS}}[\text{CoO}_2]_{1.69}$ cobaltite by chimie douce methods. *J. Solid State Chem.* **183**, 1252–1257 (2010)
 35. M.A. Madre, Sh. Rasekh, K. Touati, C. Salvador, M. Depriester, M.A. Torres, P. Bosque, J.C. Diez, A. Sotelo, From nanosized precursors to high performance ceramics: the case of $\text{Bi}_2\text{Ca}_2\text{Co}_{1.7}\text{O}_x$. *Mater. Lett.* **191**, 14–16 (2017)
 36. H. Itahara, C. Xia, J. Sugiyama, T. Tani, Fabrication of textured thermoelectric layered cobaltites with various rock salt-type layers by using $\beta\text{-Co}(\text{OH})_2$ platelets as reactive templates. *J. Mater. Chem.* **14**, 61–66 (2004)
 37. E. Guilmeau, M. Mikami, R. Funahashi, D. Chateigner, Synthesis and thermoelectric properties of $\text{Bi}_{2.5}\text{Ca}_{2.5}\text{Co}_2\text{O}_x$ layered cobaltites. *J. Mater. Res.* **20**, 1002–1008 (2005)
 38. B. Ozkurt, M.A. Madre, A. Sotelo, M.E. Yakinci, B. Ozcelik, Relationship between growth speed, microstructure, mechanical and electrical properties in $\text{Bi-2212}/\text{Ag}$ textured composites. *J. Supercond. Nov. Magn.* **25**, 799–804 (2012)

Publisher's Note Springer Nature remains neutral with regard to jurisdictional claims in published maps and institutional affiliations.